Launching Efficiency of the HE_{11} Surface-Wave Mode on a Dielectric Tube

GAR LAM YIP, MEMBER, IEEE, AND TATYAN AUYEUNG

Abstract—**A theoretical investigation into the launching of dipolar surface waves on a dielectric tube is presented. The source under consideration is a transversely oriented point electric dipole situated on the axis of the tube. It is found that the source excites only the dominant HE_{11} mode when the outer radius of the tube is sufficiently small. Phase and group characteristics as well as some field distributions are given for the source-free case; however, these are independent of the choice of the source, and are dependent only on the particular mode being excited. Surface-wave as well as radiated powers are obtained in terms of the current in the source dipole, and the launching efficiency of the surface waves is determined as a function of the tube radius, wall thickness, and permittivity of the material. Finally, comparisons are made between the dielectric tube and the solid rod which was investigated previously [7] as possible surface-wave transmission lines, and also the launching efficiencies for these two cases.**

I. Introduction

THE SUBJECT of dielectric surface waveguides has been receiving attention for quite some time. More recently, the demand for wider bandwidths for communication purposes has prompted research into the possible use of dielectric surface waveguides for long distance telecommunication links at the millimetric and optical frequencies [1]. Kharadly and Lewis [2] studied the propagation characteristics of a dielectric tube waveguide in the millimeter-wave region and proposed a practical system consisting of such tubes embedded in polyfoam. Sugi and Nakahara [3] suggested the use of the *O* guide and the *X* guide as possible low-loss transmission lines and Nakahara and Kurauchi [4] have mentioned applications of these structures to railroad communications at the higher microwave frequencies. At optical frequencies, Kao and Hockham [5] investigated the solid dielectric fiber but suggested the use of a cladded structure for better mechanical strength and easier handling without affecting wave propagation.

The above brief review is not intended to be exhaustive. A much more extensive bibliography on dielectric surface waveguides can be found in a review paper by Kao [1]. It appears that so far the problems of excitation of surface waves on dielectric waveguides have been studied to a much less extent. The launching of the dominant HE_{11} mode on cylindrical dielectric waveguides is particularly important because it is the easiest one to excite and the most widely used. Some experimental work was recently carried out by McRitchie and Beal [6] to launch the HE_{11} surface waves on a dielectric image line by means of a finite Yagi–Uda array of transversely oriented monopoles. Yip [7] investigated theoretically the launching of the HE_{11} mode on a dielectric rod by a transversely oriented point electric dipole situated on the rod axis. The point dipole can be taken as the idealized form of a short dipole, and, as such, the solution obtained can be regarded as the first step towards that for the more general and much more difficult case of a dipole with a finite length.

The present paper provides a theoretical investigation of the launching of the HE_{11} surface-wave mode on a dielectric tube by extending the analysis used previously for the dielectric rod [7]. Phase and group velocities are computed, and the surface-wave power and the radiated power are determined in terms of the current density on the source. The launching efficiency is then evaluated from the ratio of surface-wave to total power delivered by the dipole. Finally, comparisons are made between the propagation characteristics and the surface-wave as well as radiated powers for the dielectric tube and those for the dielectric rod. The computations have been carried out in the millimetric frequency region. However, they can be easily extended into the optical frequency region by a change of the physical parameters.

II. Formulation of the Problem

Let us consider an infinitely long cylindrical dielectric tube in free space. The inner and outer radii of this dielectric tube are given by a and b, respectively, and $c = a/b$. The three regions so defined are labeled I, II, and III. The cylindrical coordinate system (ρ,ϕ,z) is used where the z axis coincides with the tube axis, ρ is the radial distance, and ϕ the azimuthal angle. Regions I and III represent free space with permittivity ϵ_0 and permeability μ_0. Region II is assumed to be lossless dielectric characterized by a permittivity $\epsilon_2 = \epsilon_0\epsilon$ and a permeability μ_0 equal to that of free space. A point electric dipole is placed at the origin of the cylindrical coordinate system with its axis pointing in the $\phi = 0°$ direction perpendicular to the axis of the tube. We set up Maxwell's equations for the fields having a time dependence $e^{-i\omega t}$ for the three regions, and use the same Fourier transform technique as in the previous paper on the dielectric rod [7]. This

Manuscript received November 7, 1972; revised July 2, 1973. This work was supported by the National Research Council of Canada under Grant A-4411.

G. L. Yip is with the Department of Electrical Engineering, McGill University, Montreal, P. Q., Canada.

T. Auyeung was with the Department of Electrical Engineering, McGill University, Montreal, P. Q., Canada. He is now with the Antenna Laboratory, RCA Limited, Montreal, P. Q., Canada.

technique involves expressing the source and fields in a Fourier integral in the z direction and a Fourier series in the ϕ direction. Thus equations (Y1)–(Y7) (Y is used to indicate that reference is made to [7]) remain valid for the present case except that the permittivity ϵ for the rod should now be replaced by ϵ_0 for the region I. The transverse fields are expressed in terms of the longitudinal fields in (Y6) and the wave equations for the longitudinal fields in (Y7) are also valid in regions II and III if the permeability and permittivity in each region are appropriately taken care of, and the source terms in (Y7) are dropped. The transformed longitudinal field solutions can be written as follows. In region I,

$$H_{z1,m}(\rho,\gamma) = I\eta_0[S_m H_1^{(1)}(k_0\eta_0\rho) + B_m J_1(k_0\eta_0\rho)] \quad (1a)$$

$$iE_{z1,m}(\rho,\gamma) = I\eta_0[T_m H_1^{(1)}(k_0\eta_0\rho) + A_m J_1(k_0\eta_0\rho)]. \quad (1b)$$

In region II,

$$H_{z2,m}(\rho,\gamma) = I\eta[C_m Y_1(k_0\eta\rho) + D_m J_1(k_0\eta\rho)] \quad (2a)$$

$$iE_{z2,m}(\rho,\gamma) = I\eta[E_m Y_1(k_0\eta\rho) + F_m J_1(k_0\eta\rho)]. \quad (2b)$$

In region III,

$$H_{z3}(\rho,\gamma) = IG_m H_1^{(1)}(k_0\eta_0\rho) \quad (3a)$$

$$iE_{z3}(\rho,\gamma) = IL_m H_1^{(1)}(k_0\eta_0\rho) \quad (3b)$$

where $I = i(J_e/4)(\mu_0)^{1/2}$, $T_m = i\gamma/2$, $S_m = -im/2$, $m = 1$ and -1, $\eta_0 = (1-\gamma^2)^{1/2}$, $\eta = (\epsilon - \gamma^2)^{1/2}$, k_0 is the wavenumber in free space, γ is the Fourier transform variable, and $A_m, B_m, \cdots, L_m$ are unknown coefficients to be determined. An angular dependence factor of $e^{im\phi}$ and a time dependence factor of $e^{-i\omega t}$ have been omitted from the above field expressions.

The eight coefficients can be determined through the imposition of the boundary conditions, which require continuity of the tangential components of the electric and magnetic fields $(E_\phi, H_\phi, E_z, H_z)$ across the two dielectric–air interfaces. The application of such boundary conditions thus lead to eight simultaneous equations in the eight unknown coefficients, the complete form of which is given in the Appendix. It can be written as

$$[Q][X] = [S]. \quad (4)$$

The unknown coefficients contained in X can be solved systematically using Cramer's rule. The determinant of $[Q]$ can be expressed as $F_s\Delta(\gamma)$, where F_s is a certain factor and $\Delta(\gamma)$ will be shown to be the dispersion equation for the surface waves on the dielectric tube. The coefficients can thus be conveniently expressed as $A_m = \bar{A}_m/\Delta(\gamma)$, $B_m = \bar{B}_m/\Delta(\gamma)$, $\cdots$, etc.

We have now obtained a complete description of the transformed fields in terms of the source current. The actual fields can be obtained by Fourier transformation, e.g.,

$$H_{z1}(\rho,\phi,z) = \frac{k_0}{2\pi}\int_{-\infty}^{\infty} H_{z1}(\rho,\phi,\gamma)e^{ik_0\gamma z}\,d\gamma \quad (5)$$

where

$$H_{z1}(\rho,\phi,\gamma) = \sum_{m=-1,1} I\eta_0[S_m H_1^{(1)}(k_0\eta_0\rho) + B_m J_1(k_0\eta_0\rho)]e^{im\phi}. \quad (6)$$

The Fourier integral can be evaluated by means of a contour integration as discussed in some detail in the previous paper on the dielectric rod. It is emphasized that the transversely oriented dipole considered here excites fields with azimuthal variations exp $(\pm i\phi)$ only.

III. Excitation of the HE_{11} Surface-Wave Mode on a Dielectric Tube

The excitation of surface waves and space waves in the present problem is much the same as in the case of the dielectric rod [7]. Briefly speaking, the total field is produced by the contributions from the branch cut integral, giving rise to space waves, as well as the residues at the real poles of the integrand, giving rise to surface waves. The space waves, which represent radiation loss, will be discussed later. The real poles correspond to the zeros of $\Delta(\gamma)$, since $B_m = \bar{B}_m/\Delta(\gamma)$. Hence, $\Delta(\gamma) = 0$ yields the dispersion equation of the surface waves on a dielectric tube. The dispersion characteristics for the various surface-wave modes have been studied by several investigators (e.g., [8], [9]). The most recent and detailed study is perhaps that of Kharadly and Lewis [2]. When the outer radius b is sufficiently small, only the dominant HE_{11} mode will be excited. The dispersion characteristics of the HE_{11} mode are presented here for the sake of discussion.

In Fig. 1(a), the normalized phase velocity $(1/\gamma)$ of the HE_{11} mode is plotted versus the normalized external tube radius (b/λ_0), λ_0 being the wavelength in free space. The HE_{11} mode exhibits no low-frequency cutoff, and at large values of (b/λ_0), the normalized phase velocity approached $1/\epsilon^{1/2}$, the velocity of propagation of a plane wave in an infinite medium of permittivity ϵ. The curves show that increasing the wall thickness (reducing c) has the effect of reducing the phase velocity of the HE_{11} mode. By subjecting c to sufficiently small values in $\Delta(\gamma) = 0$ ($c = 0.0005$, say), dispersion characteristics for the solid rod can be recovered to check with published results. For single-mode operation, where only the dominant HE_{11} mode is used, the tube radii must be small enough to be below the cutoff points for the next higher order mode, the H_{01} mode. The latter have been computed with the formula developed by Kharadly and Lewis [2] and with the set of parameters used for the HE_{11} mode as shown in Table I. Since $\gamma = 1$ at cutoff, we can see from the last column in Table I that there is an appreciable difference in the phase velocities of the HE_{11} and H_{01} modes at the cutoff of the latter.

The group velocity can be found by determining the rate of energy transport in the direction of the axis of the guide. However, a novel way was used. The method involves differentiating the characteristic equation. This

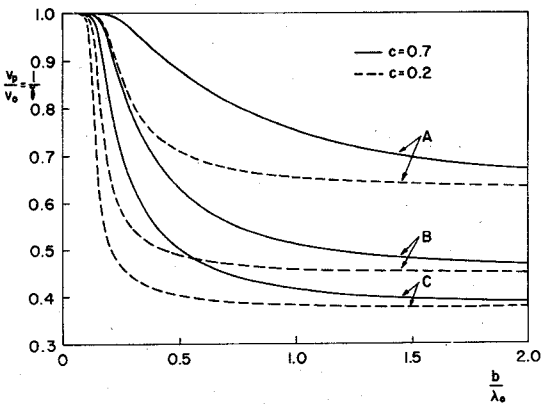

(a)

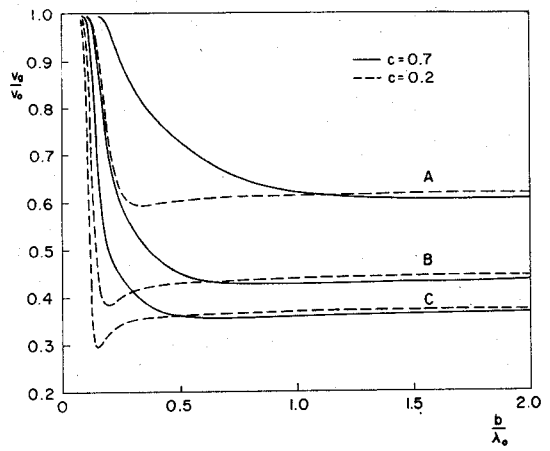

(b)

Fig. 1. (a) Dispersion characteristics of the HE_{11} mode on a dielectric tube. A: $\epsilon = 2.56$; B: $\epsilon = 5$; C: $\epsilon = 7.12$. (b) Normalized group velocities of the HE_{11} mode on a dielectric tube. A: $\epsilon = 2.56$; B: $\epsilon = 5$; C: $\epsilon = 7.12$.

TABLE I

ϵ	c	b/λ_0 at cutoff of H_{01} mode	v_p/v_0 of HE_{11} mode
2.56	0.7	0.3776	0.925
	0.2	0.3070	0.805
5.00	0.7	0.2358	0.875
	0.2	0.1918	0.835
7.12	0.7	0.1906	0.690
	0.2	0.1550	0.635

method was chosen because the characteristic equation has to be differentiated in a latter part of the work to evaluate the surface-wave power, where field components of the surface waves are evaluated by using the residue theory.

$$\frac{1}{v_g} = \frac{d\beta}{d\omega} = \frac{1}{v_0}\left[\gamma + k_0 \frac{d\gamma}{dk_0}\right].$$

Hence

$$\frac{v_g}{v_0} = \frac{1}{v_0}\frac{d\omega}{d\beta} = \frac{1}{\gamma + (1/x)} \tag{7}$$

where

$$x = \frac{1}{k_0}\frac{dk_0}{d\gamma}.$$

By differentiating the characteristic equation $\Delta(\gamma) = 0$ with respect to γ, we obtain an equation in x, which can be solved in the same way as γ itself. This value of x can then be substituted in (7) to obtain the normalized group velocity. Plots of v_g/v_0 against b/λ_0 are shown in Fig. 1(b). The normalized group velocity also approaches that of a TEM wave in medium II when b/λ_0 is increased. A phenomenon not observed in the phase characteristics is that b/λ_0, the normalized group velocity, falls below the value of $1/\epsilon^{1/2}$. The rate of change of group velocity with external radius becomes increasingly rapid for a thick tube with high permittivity. It becomes zero at some value of b/λ_0 depending on ϵ and c and begins to change sign until it reaches almost zero again at large b/λ_0. The above formulation of the group velocity from the derivative of the characteristic equation has been found to yield results which agree with those obtained by Kharadly and Lewis, who used the rate of energy transport approach.

IV. The Surface-Wave Power in the HE_{11} Mode

The power carried by surface waves in the positive z direction in region i is given by

$$P_{si} = \frac{1}{2(\mu_0\epsilon_0)^{1/2}} \operatorname{Re} \int_0^{2\pi} \int_\rho [E_{\rho i}(\rho,\phi,z) H_{\phi i}^*(\rho,\phi,z) - E_{\phi i}(\rho,\phi,z) H_{\rho i}^*(\rho,\phi,z)] \rho d\rho d\phi \tag{8}$$

where $\int_\rho$ is taken between o and a in region I, between a and b in region II, and between b and ∞ in region III.

By symmetry, the total surface-wave power is twice that carried in the positive z direction, i.e.,

$$\bar{P}_s = 2(P_{s1} + P_{s2} + P_{s3}).$$

This can be normalized with respect to the source current according to

$$\bar{P}_s = \frac{J_e^2}{2} P_s \tag{9}$$

where P_s is the normalized power. Plots of P_s are presented as a function of b/λ_0 in Fig. 2(a) and (b), and as a function of c for $c = 0.2$ and 0.7 in Fig. 3(a) and (b). For applications in the millimetric frequency region, the operating wavelength is taken to be 8 mm. It is seen that in each case, there is a maximum value of P_s which can be achieved by a proper choice of b/λ_0 for a fixed ϵ and vice versa. From Fig. 2(a) and (b), it is evident that the maximum P_s is attained at a value of b/λ_0 below the cutoff point for the next higher order mode, i.e., H_{01} mode for practically all the cases. For a particular dielectric material, maximum power occurs at a relatively small external radius of the tube (b/λ_0 less than 0.3 in all cases under consideration). This is a desirable feature both from the point of view of single-mode operation and

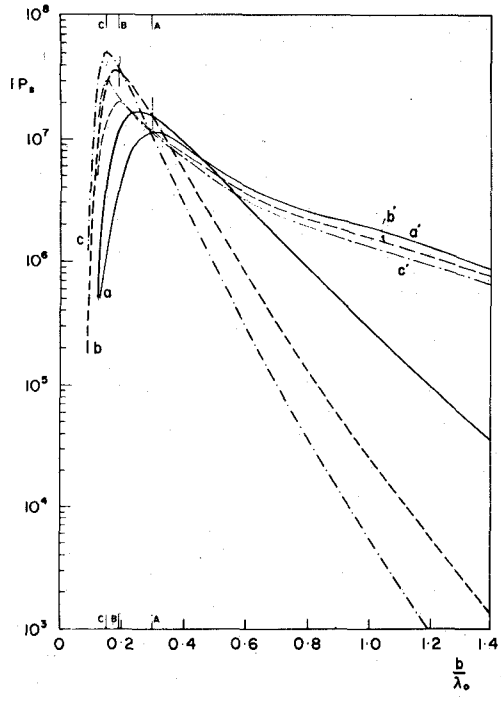

(a)

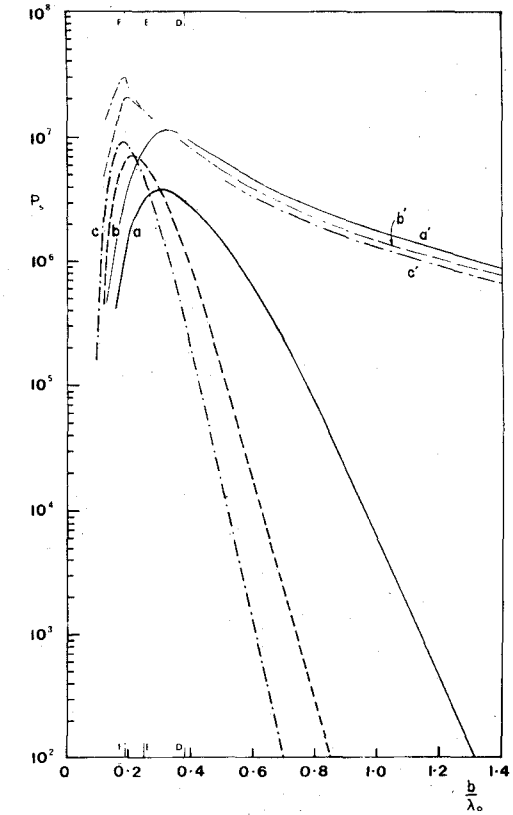

(b)

Fig. 2. Normalized surface-wave power. (a) P_s as a function of b/λ_0: $c = 0.2$. *a*) $\epsilon = 2.56$; *b*) $\epsilon = 5$; *c*) $\epsilon = 7.12$. *A*, *B*, *C* are the cutoff points for the H_{01} mode for $\epsilon = 2.56$, 5, and 7.12, respectively. *a'*, *b'*, and *c'* refer to the dielectric rod. (b) P_s as a function of b/λ_0: $c = 0.7$. *a*) $\epsilon = 2.57$; *b*) $\epsilon = 5$; *c*) $\epsilon = 7.12$. *D*, *E*, *F* are the cutoff points for the H_{01} mode for $\epsilon = 2.56$, 5, and 7.12, respectively. *a'*, *b'*, *c'* refer to the dielectric rod.

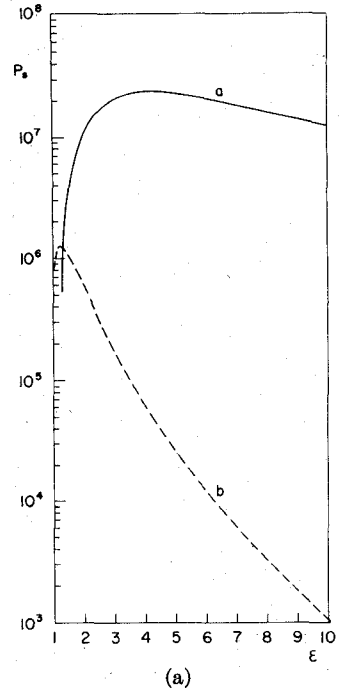

(a)

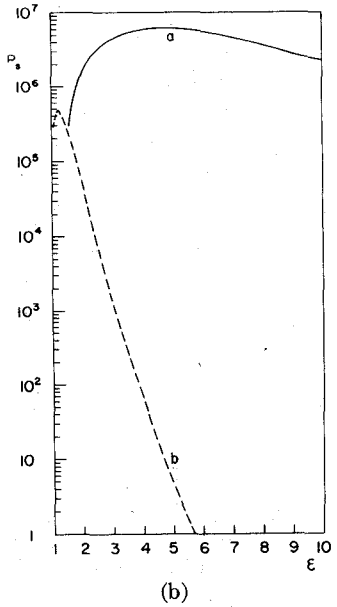

(b)

Fig. 3. Normalized surface-wave power. (a) P_s as a function of ϵ: $c = 0.2$. *a*) $b/\lambda_0 = 0.25$; *b*) $b/\lambda_0 = 1$. (b) P_s as a function of ϵ: $c = 0.7$. *a*) $b/\lambda_0 = 0.25$; *b*) $b/\lambda_0 = 1$.

material cost. Also, at such a low value of b/λ_0, the power changes very slowly with respect to the dielectric constant of the material [Fig. 3(a) and (b)]. For a thick tube ($b/\lambda_0 = 1$), the surface-wave power decreases very rapidly with ϵ after reaching a sharp maximum at ϵ slightly greater than unity. For ϵ arbitrarily close to 1 or b/λ_0 approaching zero, P_s is expected to drop to zero irrespective of the value of c because, in these cases, an interface does not exist to guide the surface waves.

In addition to the above observations, it can also be seen that for the same values of ϵ and b/λ_0, a thicker tube (c small) carries a larger amount of power than a thin

one. The maximum power is increased by a factor of approximately 5 for all three permittivities when c is reduced from 0.7 to 0.2. A comparison with the case of the rod [7] reveals that the surface-wave power characteristics of the rod lie somewhat in between these two plots for the tube. The value of c thus provides an additional design parameter not available in the solid rod. By making the wall of the tube sufficiently thick while maintaining a tiny air space at the core, the surface-wave power can be made to exceed that of the rod. It can be shown that the results here for the tube do not converge to those for the rod when we put c arbitrarily close to zero. There exists a finite ratio between the surface-wave power of a solid rod and that of a tube with its c approaching zero. This ratio, which depends on ϵ, will be discussed in the next section.

V. Space Waves and the Launching of the HE_{11} Mode

The power in the space waves excited by the dipole can be evaluated in a similar manner as was done previously for the case of the solid dielectric rod [7]. Briefly speaking, the space-wave power can be determined by integrating the real part of the radial component of the complex Poynting vector in region III over a cylindrical surface of radius ρ greater than the outer radius b of the dielectric tube. By introducing the transformed field quantities and applying Parseval's theorem, the final expression for the total power P_r radiated in the form of space waves can be shown to be given by

$$P_r = \frac{J_e^2}{2}\left(\frac{\mu_0}{\epsilon_0}\right)^{1/2}\frac{k_0^2}{4\pi}\sum_{m=1,-1}\int_0^1 [|G_m|^2 + |L_m|^2]\,d\gamma \quad (10)$$

$$= \frac{J_e^2}{2} R_r \quad (11)$$

where R_r is defined as the radiation resistance.

The integral in (10) can be evaluated numerically on a computer and the radiation resistance is then plotted as a function of b/λ_0 and ϵ with $c = 0.2$ and 0.7 and an operating wavelength of 8 mm in Fig. 4(a) and (b) and Fig. 5(a) and (b). The oscillatory phenomenon observed in these plots can be attributed to the setting up of standing waves inside the dielectric tube, which also happens in the case of the dielectric rod. When the primary waves excited by the dipole reach any of the two dielectric–air interfaces, they are partly transmitted and partly reflected. The transmitted waves which eventually pass through the second interface account for the radiation fields. The reflected waves, on the other hand, interact either constructively or destructively with the incident waves to set up a standing wave pattern inside the tube. This pattern will change with either a variation in b/λ_0 or ϵ, resulting in the oscillatory behavior of the radiated power. To give an approximate quantitative prediction of the standing wave pattern, let us examine the integral in (10). For the space

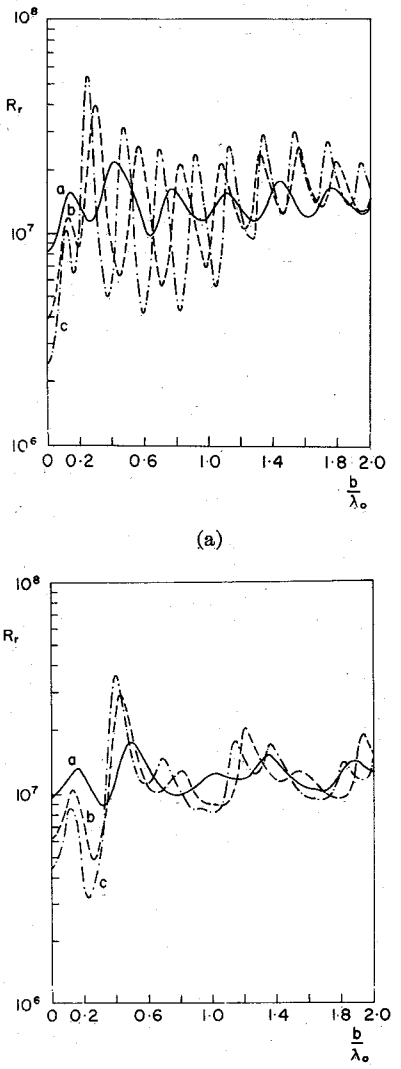

Fig. 4. Normalized radiated power. (a) R_r as a function of b/λ_0: $c = 0.2$. *a*) $\epsilon = 2.56$; *b*) $\epsilon = 5$; *c*) $\epsilon = 7.12$. (b) R_r as a function of b/λ_0: $c = 0.7$. *a*) $\epsilon = 2.56$; *b*) $\epsilon = 5$; *c*) $\epsilon = 7.12$.

waves $k_0\gamma$ represents the axial wavenumber, and $k_0\eta$ the radial wavenumber. Thus γ, which varies from 0 to 1, gives rise to an angular spectrum of cylindrical waves. We make the approximation that γ^2 be much smaller than ϵ so that $k_0\eta \simeq k_0(\epsilon)^{1/2}$ for all these waves. For thick tubes, e.g., $c = 0.2$, the tiny air column can also be neglected. Thus $k_0\eta$ causes standing waves and we should expect that two adjacent maxima be separated a distance $\lambda/2$ apart, where $\lambda = \lambda_0/\epsilon^{1/2}$ is the wavelength in the dielectric tube and λ_0 is the wavelength in free space.

Take an example of $b/\lambda_0 = 1.8$ and $\lambda_0 = 8$ mm. One should expect approximately six maxima for $\epsilon = 2.56$ and eight maxima for $\epsilon = 5$. This prediction is indeed borne out by the curves in Fig. 4(a). The above quantitative prediction can also be applied to the case of the dielectric rod, where the agreement has been verified [7, fig. 5(a)].

By letting the ratio of inner-to-outer radii of the tube approach zero, the hollow tube becomes physically close

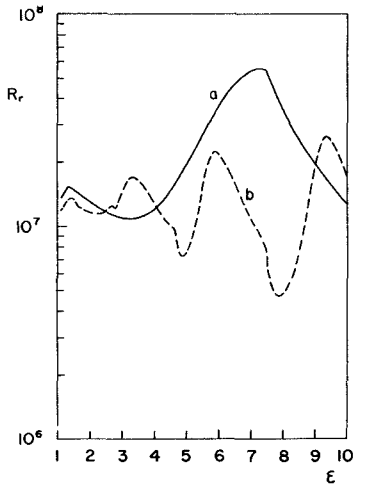

(a)

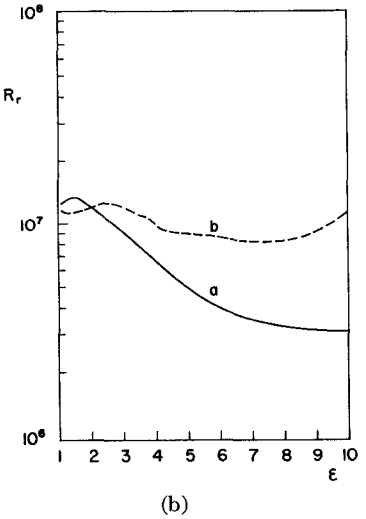

(b)

Fig. 5. Normalized radiated power. (a) R_r as a function of ϵ: $c = 0.2$. *a*) $b/\lambda_0 = 0.25$; *b*) $b/\lambda_0 = 1$. (b) R_r as a function of ϵ: $c = 0.7$. *a*) $b/\lambda_0 = 0.25$; *b*) $b/\lambda_0 = 1$.

to the solid rod. It is interesting to compare the results obtained this way with those obtained by Yip [7] for the dielectric rod. In view of the complexity of the mathematical expressions involved, we seek a simpler version of the problem by comparing the results between a small tube (b/λ_0 small) with an arbitrarily thick wall (c small) and a thin rod. By using small argument approximations of the various Bessel functions, it can be shown that

$$\frac{R_{r(\text{tube})}}{R_{r(\text{rod})}} = \frac{16\epsilon^2(1+\epsilon)^2}{[(1-c^2)^2(1+\tilde{G})(1+2\epsilon\tilde{G}+\epsilon^2)]^2}. \tag{12}$$

This ratio, which depends on ϵ and c, has been verified on a computer by putting $c = 0.0005$ in (11) and comparing the results for $\epsilon = 2.56$, 5, and 7.12 with those obtained for the rod [7]. Since the full expression for R_r has been used in computation, it appears, therefore, (12) is not limited to thin structures. In fact, this ratio has been verified up to a value of $b/\lambda_0 = 2$ for all three ϵ's.

The nonconvergence of results between a tube with c and a solid rod can be explained by examining the source conditions. For the tube problem, the source condition at $\rho = 0$ can be satisfied only when $T_m = i(\gamma/2)$ and $S_m = -(im/2)$, whereas for the rod problem $T_m = i\gamma/2\epsilon$ and $S_m = -(im/2)$. The resulting fields are therefore different in the two cases even if c is set to very small values. Further, in the present tube problem, it is specified that the electric dipole is contained within the air column ($\rho < a$) marked as region I. It follows that, in comparing the results between a tube with small c and a rod, c should not be set to zero for the field solutions in (1) to be valid. If c were zero, the source condition for the rod problem must be used. It was mentioned in the last section that the same ratio also appears when a similar comparison is made for the surface-wave power P_s. This can be expected since the field expressions for the surface waves and the space waves are identical except that the ranges of values of γ for the two types of waves are different. Since ϵ is greater than one, we see that the ratio of tube-to-rod radiated powers is always greater than unity. Thus there is a general enhancement of the surface-wave power as well as the radiated power when a thick tube is used instead of a rod.

As a check on the correctness of the results, ϵ was set to unity in (11). After much algebra, it was found that this formula yielded $R_r = 20k_0^2$, corresponding to the radiation resistance of a dipole in free space. Such verification has also been carried out for the solid rod, and it is interesting to note that for $\epsilon = 1$, (12) gives the ratio of $R_{r(\text{tube})}$ to $R_{r(\text{rod})}$ as unity.

The launching efficiency $\mathcal{E}$ of the surface waves is defined as $\mathcal{E} = P_s/(P_s + P_r)$, i.e., the proportion of the surface-wave power in relation to the total power excited by the dipole. The efficiency is presented in Fig. 6(a) and (b) and Fig. 7(a) and (b). By a proper choice of dielectric material, tube radius, and wall thickness, high efficiencies close to 80 or 90 percent can be achieved [see curves *b* and *c* in Fig. 6(a)]. It also appears that a smaller tube (b/λ_0 small) having a thick wall (c small) and a high permittivity (ϵ large) can be used to attain even higher efficiences. A large tube (b/λ_0 large), on the other hand, is a highly inefficient surface-wave carrier irrespective of the choice of ϵ and c. In most cases, the maximum launching efficiencies are attained at values of b/λ_0 below the cutoff points for the next higher order mode H_{01} on the dielectric tube. This means that by making the radius of the tube sufficiently small to ensure single-mode operation, we can achieve not only an economy in material but also high launching efficiencies for the surface waves.

VI. Conclusion

A theoretical investigation of the launching of the dominant HE_{11} mode on a dielectric tube by means of a transversely oriented electric dipole situated on the tube axis has been presented, by using the same mathematical

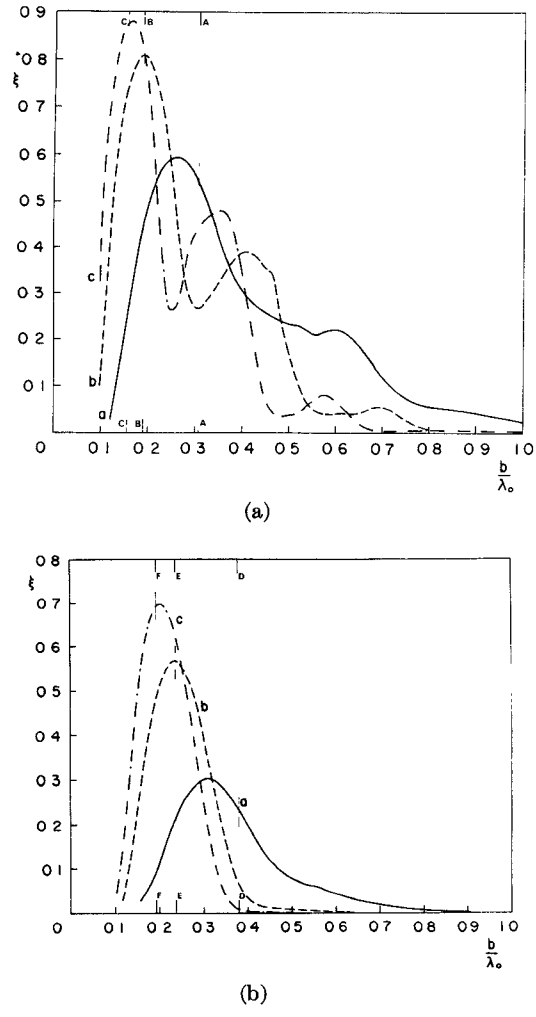

Fig. 6. (a) Launching efficiency $\mathcal{E}$ of the HE_{11} mode as a function of b/λ_0: $c = 0.2$. *a*) $\epsilon = 2.56$; *b*) $\epsilon = 5$; *c*) $\epsilon = 7.12$. *A*, *B*, *C* are as explained in Fig. 2(a). (b) Launching efficiency $\mathcal{E}$ of the HE_{11} mode as a function of b/λ_0: $c = 0.7$. *a*) $\epsilon = 2.56$; *b*) $\epsilon = 5$; *c*) $\epsilon = 7.12$. *D*, *E*, *F* are as explained in Fig. 2(b).

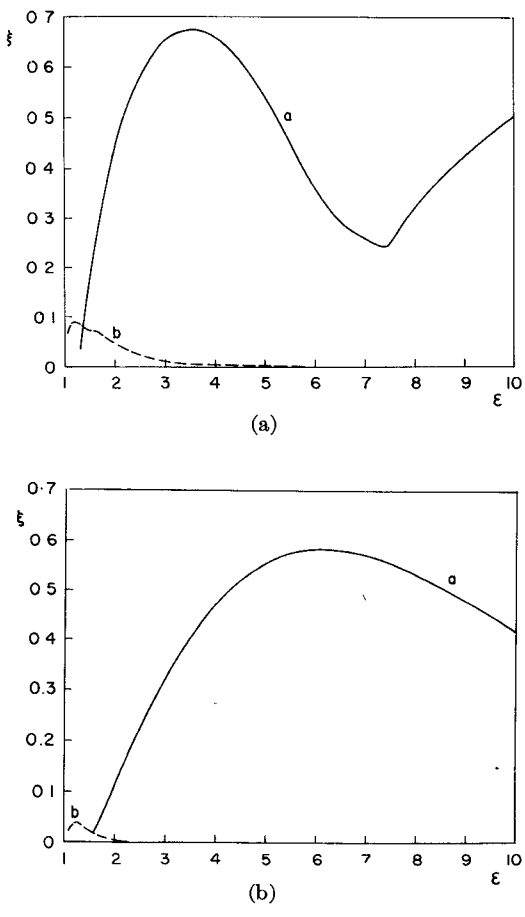

Fig. 7. (a) Launching efficiency $\mathcal{E}$ of the HE_{11} mode as a function of ϵ: $c = 0.2$. *a*) $b/\lambda_0 = 0.25$; *b*) $b/\lambda_0 = 1$. (b) Launching efficiency $\mathcal{E}$ of the HE_{11} mode as a function of ϵ: $c = 0.7$. *a*) $b/\lambda_0 = 0.25$; *b*) $b/\lambda_0 = 1$.

technique as for the dielectric rod [7]. Although the geometry of the problem has been simplified to facilitate analytical solution, this is not without its practical justifications. In fact, one of the simplest and easiest methods of exciting the dipolar mode involves feeding a dipole in front of a metallic cap attached to one end of the dielectric tube [10]. In McRitchie and Beal's experiment [6] the launching was achieved by means of a longitudinal Yagi–Uda monopole array embedded in a dielectric image line. The driven element, together with its image, constituted a transversely oriented electric dipole of finite length. Thus it is easily seen that the problem of the point dipole considered in the present work forms the first but important step towards a theoretical analysis of the launching problem. The information obtained is believed useful in design considerations for dielectric tube waveguides, surface-wave launchers, and detectors.

The surface waves on a dielectric tube have higher phase and group velocities than those on a dielectric rod of the same radius [7]. Since attenuation increases with a decrease of phase velocity [2], it is more desirable to use a thin tube with a small external radius so that the phase velocity is higher and the attenuation lower. This is also advantageous since the maximum launching efficiency occurs at a small radius of the tube. The transverse dimensions can be so chosen as to permit only the dominant HE_{11} mode to propagate.

There is yet another advantage of the dielectric tube over the rod. Since dielectric materials are lossy, it is generally more convenient to have the major portion of the fields propagating in the free-space region surrounding a dielectric waveguide. This can be achieved by using very small guides, when the normalized propagation coefficient γ is very close to unity. Unfortunately, there is no convenient way of supporting a very thin rod. With a hollow dielectric tube, a more rigid structure having a larger external radius can be used to give the same value of γ and hence support a loosely bound wave. The parameters are chosen to ensure operation above the so called

practical cutoff of the HE_{11} mode, the point where γ becomes very close to 1, so that slight discontinuties and nearby objects do not cause severe radiation losses.

Despite the above advantages of a thin tube, it appears that a thick tube (c small) gives better launching efficiencies than a thin one. For example, with $\epsilon = 2.56$ and $b/\lambda_0 = 0.25$, the efficiency is 59 percent for a tube with $c = 0.2$, and only 24 percent for one with $c = 0.7$. The maximum efficiency which can be achieved in each case is 59 and 30 percent, respectively. Hence, there is a compromise to be made between attenuation, which is lower for a thin tube, and launching efficiency, which is higher for a thick tube.

The calculations performed in the present work are primarily aimed at millimeter frequencies. An extension into the optical frequency range can be readily done by using the formulas presented in this paper. At optical frequencies, the transverse electric dipole can be considered as representing the focused spot of a light beam. Since the dimensions of the tube have been normalized with respect to the free-space wavelength, these calculations are expected to produce the same general behavior as predicted here at optical frequencies. The method of analysis can be applied readily to the case of the cladded fiber, which is a more practical transmission line at optical frequencies.

Appendix

Complete Form of (4): $[Q][X] = [S]$

$$
[Q] = \begin{bmatrix}
\eta_0 J_1(cN) & -\eta Y_1(cV) & -\eta J_1(cV) & 0 & 0 & 0 & 0 & 0 \\
0 & 0 & 0 & 0 & \eta_0 J_1(cN) & -\eta Y_1(cV) & -\eta J_1(cV) & 0 \\
\frac{\gamma m}{\eta_0 a} J_1(cN) & \frac{-\gamma m}{\eta a} Y_1(cV) & \frac{-\gamma m}{\eta a} Y_1(cV) & 0 & -k_0 J_1'(cN) & k_0 Y_1'(cV) & k_0 J_1'(cV) & 0 \\
k_0 J_1'(cN) & -\epsilon k_0 Y_1'(cV) & -\epsilon k_0 J_1'(cV) & 0 & \frac{-\gamma m}{\eta_0 a} J_1(cN) & \frac{\gamma m}{\eta a} Y_1(cV) & \frac{\gamma m}{\eta a} J_1(cV) & 0 \\
0 & \eta Y_1(V) & \eta J_1(V) & -\eta_0 H_1^{(1)}(N) & 0 & 0 & 0 & 0 \\
0 & 0 & 0 & 0 & 0 & Y_1(V) & \eta J_1(V) & -\eta_0 H_1^{(1)}(N) \\
0 & \frac{-\gamma m}{\eta b} Y_1(V) & \frac{-\gamma m}{\eta b} J_1(V) & \frac{\gamma m}{\eta_0 b} H_1^{(1)}(N) & 0 & k_0 Y_1'(V) & k_0 J_1'(V) & -k_0 H_1^{(1)\prime}(N) \\
0 & -\epsilon k_0 Y_1'(V) & -\epsilon k_0 J_1'(V) & k_0 H_1^{(1)\prime}(N) & 0 & \frac{\gamma m}{\eta b} Y_1(V) & \frac{\gamma m}{\eta b} J_1(V) & \frac{-\gamma m}{\eta_0 b} H_1^{(1)}(N)
\end{bmatrix}
$$

$$
[X] = \begin{bmatrix} A_m \\ E_m \\ F_m \\ L_m \\ B_m \\ C_m \\ D_m \\ G_m \end{bmatrix}
\qquad
[S] = \begin{bmatrix}
-\eta_0 T_m H_1^{(1)}(cN) \\
-\eta_0 S_m H_1^{(1)}(cN) \\
S_m k_0 H_1^{(1)\prime}(cN) - \frac{\gamma_m}{\eta_0 a} T_m H_1^{(1)}(cN) \\
\frac{\gamma_m}{\eta_0 a} S_m H_1^{(1)}(cN) - T_m k_0 H_1^{(1)\prime}(cN) \\
0 \\ 0 \\ 0 \\ 0
\end{bmatrix}
$$

References

[1] K. C. Kao, "Dielectric surface waveguides," presented at the URSI General Assembly, Ottawa, Canada, Paper 6-3.2, Aug. 18–28, 1969.
[2] M. M. Z. Kharadly and J. E. Lewis, "Properties of dielectric-tube waveguides," *Proc. Inst. Elec. Eng.*, vol. 116, pp. 214–224, Feb. 1969.
[3] M. Sugi and T. Nakahara, "O-guide and X-guide: An advanced surface wave transmission concept," *IRE Trans. Microwave Theory Tech.*, vol. MTT-7, pp. 366–369, July 1959.
[4] T. Nakahara and N. Kurauchi, "Millimeter waveguides with applications to railroad communications," in *Advances in Microwaves*, L. Young, Ed. New York: Academic, 1969, vol. 4, p. 191.
[5] K. C. Kao and G. Hockham, "Dielectric-fibre surface waveguides for optical frequencies," *Proc. Inst. Elec. Eng.*, vol. 113, pp. 1151–1158, July 1966.
[6] W. K. McRitchie and J. C. Beal, Dep. Elec. Eng., Queen's Univ., Canada, private communication.
[7] G. L. Yip, "Launching efficiency of the HE_{11} surface wave mode on a dielectric rod," *IEEE Trans. Microwave Theory Tech. (1970 Symposium Issue)*, vol. MTT-18, pp. 1033–1041, Dec. 1970.
[8] M. M. Astrahan, "Guided waves on hollow dielectric tubes," Ph.D. dissertation, Northwestern Univ., Evanston, Ill., 1949.
[9] W. C. Jakes, "Attenuation and radiation characteristics of dielectric tube waveguides," Ph.D. dissertation, Northwestern Univ., Evanston, Ill., 1949.
[10] D. G. Kiely, *Dielectric Aerials*. London: Methuen, 1953.

Systematic Design of Stacked-Crystal Filters by Microwave Network Methods

ARTHUR BALLATO, SENIOR MEMBER, IEEE, HENRY L. BERTONI, MEMBER, IEEE, AND THEODOR TAMIR, SENIOR MEMBER, IEEE

Abstract—**A class of novel frequency-selective devices, called stacked-crystal filters, is discussed in terms of a microwave network approach that leads to a systematic procedure for their analysis and design. These devices consist of two or more crystal plates that are stacked together, with thin electrodes being provided between some or all of the adjacent interfaces for the purpose of translating mechanical properties into electrical signals via piezoelectric coupling. In such a configuration, the electromechanical coupling that occurs at the plate surfaces produces selective interactions between the elastic modes in each crystal plate, as well as between these modes and all of the modes in the other plates included in a stack. A judicious combination of materials and dimensions can therefore provide a very wide range of desired filtering characteristics.**

For stacks with thin plates, only three thickness modes appear in each plate and they can be described in terms of three transmission lines; their coupling at the plate surfaces is then expressible in terms of ideal transformers that represent the mechanical junction between two adjacent plates. The interface electrodes appear as a set of terminals, to which are attached capacitors and another set of ideal transformers that represent the piezoelectric drive. In this manner, each plate can be rigorously described in terms of a well-defined network that serves as a building block. A stack consisting of any number of plates can therefore be regarded as the connection of an appropriate number of such building blocks, thus reducing a complicated mathematical problem to a systematic representation that can readily be handled by conventional techniques. A simple example of a two-layer quartz device operating on these principles is given. The simulated behavior obtained from the exact equivalent network discloses that wide-band filters may be designed. Construction of such devices can be expected to yield robust, miniature filters of high performance possessing a large diversity of desired characteristics.

Manuscript received December 20, 1972; revised June 25, 1973. The work of A. Ballato was supported by USAECOM, Ft. Monmouth, N.J. This paper is based on part of a dissertation submitted by A. Ballato to the Faculty of the Polytechnic Institute of New York, Brooklyn, N.Y., in partial fulfillment of the requirements for the Ph.D. degree in electrophysics in June 1972. The work of H. L. Bertoni and T. Tamir was supported by the Joint Services Electronics Program under Contract F44620-69-C-0047.

A. Ballato is with the U.S. Army Electronics Technology and Devices Laboratory, U.S. Army Electronics Command, Fort Monmouth, N.J. 07703.

H. L. Bertoni and T. Tamir are with the Department of Electrical Engineering and Electrophysics, Polytechnic Institute of New York, Brooklyn, N.Y. 11201 (formerly Polytechnic Institute of Brooklyn).

I. Introduction

PIEZOELECTRIC crystal plates that vibrate mechanically in response to an applied voltage have long been used as compact, rugged, very stable and low-loss one-port resonant elements in frequency-selective circuits. In this paper, a method is given for representing and analyzing a new class of bulk-wave crystal filters, which are formed by stacking two or more crystal plates with electrodes between them [1]. One can thus expect to achieve filters that take advantage of all the desirable properties of crystal plates and to exploit the diversity obtained by joining plates made of different materials. A principal contribution of this study is the development of new equivalent networks, which make possible the systematic investigation of these *stacked-crystal* filters.

The traditional crystal filter consists of an assembly of individual crystal resonators that are wired into an